# Shortened tethering filaments stabilize presynaptic vesicles in support of elevated release probability during LTP in rat hippocampus

Jae Hoon Jung[a,b], Lyndsey M. Kirk[c], Jennifer N. Bourne[c,d,1], and Kristen M. Harris[c,2]

[a]Laboratory of Neurobiology, National Institute of Neurological Disorders and Stroke, National Institutes of Health, Bethesda, MD 20892; [b]Department of Biology, Texas A&M University, College Station, TX 77843; [c]Department of Neuroscience, Center for Learning and Memory, Institute for Neuroscience, University of Texas at Austin, Austin, TX 78712; and [d]Department of Cell and Developmental Biology, University of Colorado, Aurora, CO 80045

**Long-term potentiation (LTP) is a cellular mechanism of learning and memory that results in a sustained increase in the probability of vesicular release of neurotransmitter. However, previous work in hippocampal area CA1 of the adult rat revealed that the total number of vesicles per synapse decreases following LTP, seemingly inconsistent with the elevated release probability. Here, electron-microscopic tomography (EMT) was used to assess whether changes in vesicle density or structure of vesicle tethering filaments at the active zone might explain the enhanced release probability following LTP. The spatial relationship of vesicles to the active zone varies with functional status. Tightly docked vesicles contact the presynaptic membrane, have partially formed SNARE complexes, and are primed for release of neurotransmitter upon the next action potential. Loosely docked vesicles are located within 8 nm of the presynaptic membrane where SNARE complexes begin to form. Nondocked vesicles comprise recycling and reserve pools. Vesicles are tethered to the active zone via filaments composed of molecules engaged in docking and release processes. The density of tightly docked vesicles was increased 2 h following LTP compared to control stimulation, whereas the densities of loosely docked or nondocked vesicles congregating within 45 nm above the active zones were unchanged. The tethering filaments on all vesicles were shorter and their attachment sites shifted closer to the active zone. These findings suggest that tethering filaments stabilize more vesicles in the primed state. Such changes would facilitate the long-lasting increase in release probability following LTP.**

long-term potentiation | synaptic plasticity | ultrastructure | nanoscale

Long-term potentiation (LTP) is the persistent strengthening of synapses after a brief high-frequency stimulation and is widely accepted as a cellular correlate of learning and memory (1, 2). Within minutes after the induction of LTP, new receptors are inserted into the postsynaptic membrane. The resulting increase in the excitatory postsynaptic potential is immediate and can persist for hours in vitro or days to months in vivo (1, 3–8). Quantal content is also increased soon after LTP induction and reflects an increase in the number of presynaptic vesicles that release neurotransmitter (9–13). This increase in release probability is sustained several hours following LTP (14), concurrent with postsynaptic growth and spine enlargement (15). One might expect that the enhanced probability of release would involve increasing the number of vesicles docked and primed for neurotransmitter release. However, 2 h after induction of LTP, the total number of both docked and nondocked vesicles per presynaptic bouton are markedly decreased relative to control stimulation (16). These findings raise the question of whether an altered structure of docking and priming molecules leads to local clustering of vesicles that would elevate the probability of release following LTP.

The proteins that connect synaptic vesicles to the plasma membrane can be visualized as filaments with electron-microscopic tomography (EMT) connecting vesicles to the presynaptic active zone

(17–24). Studies suggest that the SNARE complex begins to form when a vesicle and presynaptic membrane are within 8 nm of each other rendering them loosely docked (25–27). Vesicles are then drawn toward the active zone, and the SNARE complex bundle is fully formed when the vesicle is within 2 nm of the presynaptic membrane (26, 28). Tightly docked vesicles are defined as being in contact with the presynaptic membrane and correspond to primed vesicles that comprise the readily releasable pool (27). Recent studies have suggested that docked vesicles can oscillate between loosely and tightly docked states (27, 29), providing a target mechanism for synaptic plasticity.

To address the question of how changes in vesicle proximity and tethering might enhance the probability of release, we used EMT, which enabled us to acquire high-resolution structural data from small volumes of presynaptic boutons that were enriched in synaptic vesicles. We targeted active zones of hippocampal synapses, comparing their structure 2 h after LTP induction to control stimulation. The vesicle density and tethering filament dimensions were unchanged for the loosely docked and nondocked vesicles. In contrast, the density of tightly docked vesicles was increased, their tethering filaments were shorter, and the filament attachment sites on the vesicles were positioned closer to the side of the vesicle membrane facing the presynaptic membrane. Such alterations could contribute to the sustained increase in the probability of neurotransmitter release following LTP.

## Significance

Long-term potentiation (LTP), a form of synaptic plasticity important for learning and memory, results in an increased probability of release of neurotransmitter from presynaptic vesicles. Prior work showed total vesicle number was decreased following LTP, seemingly inconsistent with this increased probability of release. Presynaptic vesicles are tethered to the active zone via filaments composed of molecules engaged in docking, priming, and release processes. Here, electron-microscopic tomography revealed a higher density of docked vesicles at active zones. Tethering filaments on vesicles at the active zone were shorter, and their attachment sites were shifted closer to the active zone. These changes suggest more vesicles were docked and primed, which would increase the probability of release 2 h after induction of LTP.

NEUROSCIENCE

## Results

**Increased Density of Tightly Docked Vesicles with LTP.** We targeted vesicle-rich regions of presynaptic active zones for visualization with EMT in the rat hippocampal slice fixed 2 h following induction of LTP or control stimulation. In control (Fig. 1 *A–D*) and LTP (Fig. 1 *E–H*) conditions, vesicles located within 45 nm of the presynaptic membrane were identified and quantified with respect to distance from the plasma membrane. This distance was optimal for imaging both docked and nondocked vesicles tethered to the presynaptic membrane and captured in the same EMT image. For each EMT region, an unbiased sampling volume was represented by exclusion (red) and inclusion (green) planes through the active zone (Fig. 1 *I–L*). The contact areas of tightly docked vesicles with the presynaptic membrane are illustrated in purple on the active zone (Fig. 1 *I* and *K*). None of the tightly docked vesicles appeared to be hemifused because no pores were observed, and the bilayers were distinct between the vesicles and adjacent presynaptic membranes. The boundaries of loosely docked vesicles (dark blue), located within 8 nm of the presynaptic membrane, were also projected onto the active zone (Fig. 1 *J* and *L*). Similarly, projected boundaries of nondocked vesicles (light blue), located greater than 8 nm of the presynaptic membrane, are illustrated (Fig. 1 *J* and *L*). The density of tightly docked vesicles increased after LTP (Fig. 1*M*; Kolmogorov–Smirnov [KS] test, $P = 0.02$), whereas the densities of the loosely docked and nondocked vesicles were not significantly altered by LTP (Fig. 1*M*). Furthermore, the actual distances between loosely docked and nondocked vesicles to the presynaptic membrane were not significantly different between control and LTP conditions (Fig. 1*N*).

Prior work analyzing three-dimensional (3D) reconstructions of complete presynaptic boutons and postsynaptic surfaces showed that the total number of docked and nondocked vesicles was substantially lower 2 h following LTP (15, 16, 30). However, the vesicle docking sites were not uniformly distributed across the presynaptic membrane but appear to be congregated in clusters that define active zones where vesicles release neurotransmitter. These targeted EMT images reveal that these active zones indeed have elevated densities of tightly docked vesicles following LTP.

**Vesicle Contact Area and Presynaptic Filament Occupancy Unaltered after LTP.** The extent of contact areas between tightly docked vesicles and the presynaptic membrane could influence the probability of release. The addition of scaffolding or other active zone proteins could also influence the distribution of docking sites. Filamentous proteins surrounded presynaptic vesicles (yellow) and occupied the synaptic cleft (green) and postsynaptic surface (red) in both control (Fig. 2*A*) and LTP conditions (Fig. 2*B*). An en face view revealed the contact areas of docked vesicles (blue) and areas of filaments (yellow) that occupied the presynaptic membrane (gray, Fig. 2 *C* and *D*). The extent of filaments (red) emanating from the postsynaptic density (PSD) to contact the cytosolic face of the postsynaptic membrane (gray) are also illustrated in control (Fig. 2*E*) and LTP (Fig. 2*F*) conditions.

The contact areas of tightly docked vesicles with the presynaptic membranes did not differ significantly between synapses in the control and LTP conditions (Fig. 2 *G* and *H*). The area ratio equaled the area occupied by filaments at presynaptic or postsynaptic membranes divided by the total membrane areas (Fig. 2 *I–K*). Total presynaptic membrane area was reduced by subtracting the contact areas of tightly docked vesicles because no filaments could occur there. Under control conditions, the area occupied by filaments was comparable between the postsynaptic and presynaptic membranes (Fig. 2*I*). Following LTP, however, the filament occupancy was greater on the postsynaptic membrane than the presynaptic membrane (Fig. 2 *J* and *K*). In contrast, the proportion of the presynaptic membrane occupied by filaments was not altered by LTP (Fig. 2*K*). These findings suggest that neither the contact area nor the degree to which filaments occupy the presynaptic membrane account for the increased probability of release 2 h after LTP.

**Vesicle Tethering Filaments Shorten after LTP.** Tethering filaments on presynaptic vesicles were identified and reconstructed (Fig. 3 *A–D′*) to assess whether their structure was altered following LTP compared to control stimulation. There were 2 to 14 filaments tethering a vesicle to the presynaptic membrane (Table 1). The average number of tethering filaments per docked vesicle did not differ significantly between the LTP ($4.0 \pm 1.5$) and control ($4.1 \pm 1.6$) conditions (KS test, $P = 0.99$). Similarly, the average number of tethering filaments per nondocked (LTP, $2.5 \pm 0.69$; control, $3.4 \pm 1.8$) or loosely docked vesicle (LTP, $3.9 \pm 1.7$; control, $5.3 \pm 2.5$) was not significantly altered by LTP (KS test, $P = 0.16$ for loosely docked, and $P = 0.27$ for nondocked vesicles). Since there were no differences between LTP and control conditions in the density of loosely or nondocked vesicles at the active zone (Fig. 1) or their filament numbers, these two pools were combined for subsequent analyses of tethering filament dimensions.

A direct measure of the tethering filament length was not possible because filaments were curved or irregularly shaped. Instead, two measures were obtained for each filament (Fig. 3*E*, insets) including 1) the perpendicular distance from the filament's vesicle attachment site to the presynaptic membrane ($\text{Fil}_{VA}$–PM) and 2) the linear distance from the filament's vesicle attachment site to its attachment site on the presynaptic membrane ($\text{Fil}_{VA}$–$\text{Fil}_{PA}$). A third distance (PM–$\text{Fil}_{PA}$) was calculated assuming a right triangle between these two measures (dotted line, Fig. 3 *E*, *Insets*). All three values were on average shorter in the LTP than in the control condition for the tightly docked vesicles (Fig. 3 *E*, *Left*). For the loosely docked and nondocked vesicles, the $\text{Fil}_{VA}$–PM and $\text{Fil}_{VA}$–$\text{Fil}_{PA}$ measurements were also shorter; however, the calculated PM–$\text{Fil}_{PA}$ was not altered significantly by LTP (Fig. 3 *E*, *Right*).

The dimensions for all the filaments on each synaptic vesicle were averaged to test whether the LTP-related filament shortening was dependent on the minimum distance of the vesicle from the presynaptic membrane. For tightly docked vesicles, this distance was zero; hence, the filament averages were compared relative to the contact area of the vesicle with the presynaptic membrane (Fig. 3*F*). All three measures were uniformly shorter after LTP across all contact areas for the tightly docked vesicles (Fig. 3*F*). For the loosely docked or nondocked vesicles, all three measures were well-correlated with the absolute distance of the synaptic vesicle membrane to the presynaptic membrane of the active zone (SV–PM, Fig. 3*G*). However, only the average lengths of the $\text{Fil}_{VA}$–PM and $\text{Fil}_{VA}$–$\text{Fil}_{PA}$ were shorter after LTP and there was no significant effect on the calculated PM–$\text{Fil}_{PA}$ for longer SV–PM distances (Fig. 3*G*).

## Discussion

All vesicles congregating within 45 nm above the active zone had tethering filaments attached to the presynaptic membrane (Fig. 4). Following induction of LTP, vesicle attachment sites of tethering filaments shifted downward toward the presynaptic membrane and the filaments were shortened. The density of tightly docked vesicles increased, and their tethering filament attachment sites to the presynaptic membrane moved horizontally toward the docking site. These alterations would stabilize docked vesicles at the active zone and facilitate formation of SNARE complexes. Shortened tethering filaments on the loosely or nondocked vesicles could enhance recruitment of vesicles to docking sites at the active zone. Overall, these ultrastructural changes would support a lasting increase in the probability of release during LTP.

Induction of LTP increases both quantal content (the number of presynaptic vesicles releasing neurotransmitter) and quantal amplitude (the postsynaptic response to each vesicle released) (9–11). The increase in quantal content is maintained for as long
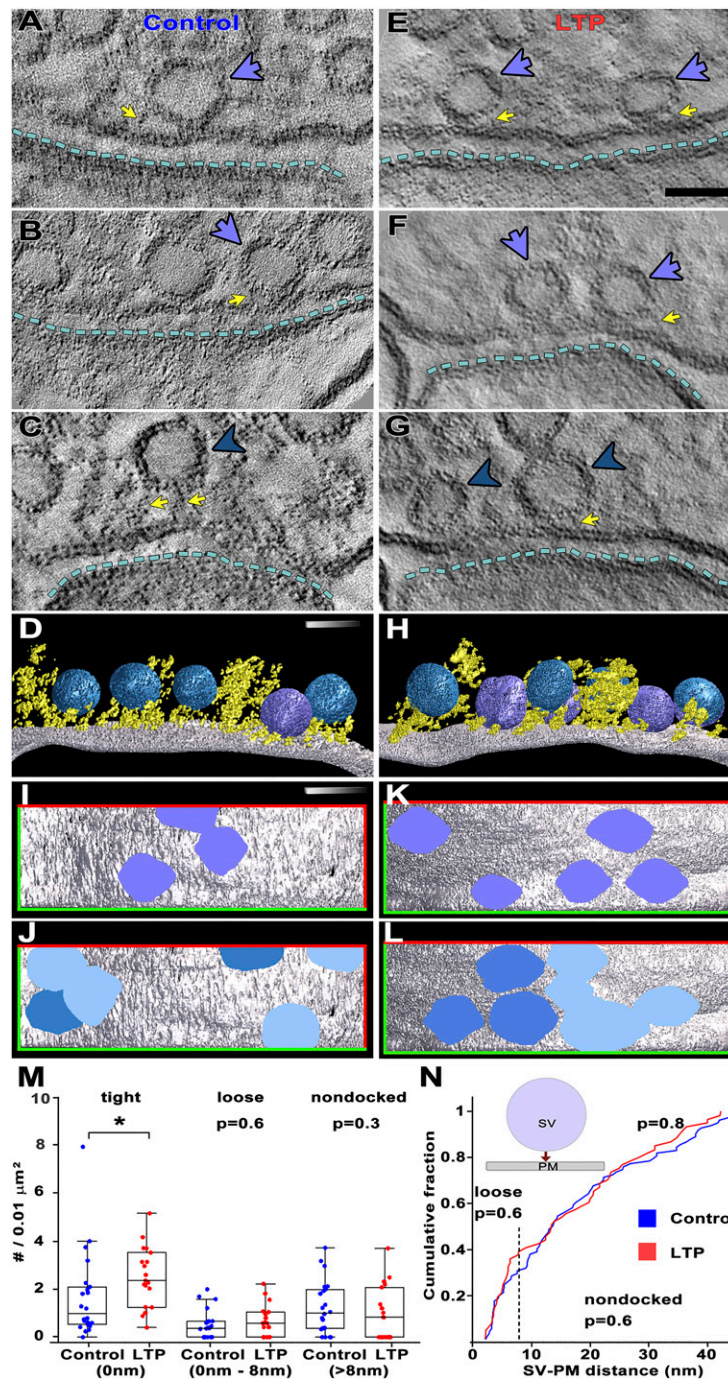
**Fig. 1.** The density of docked vesicles at presynaptic active zones increased following LTP. Virtual images and surface models of docked and nondocked vesicles within 45 nm, which are tethered by filaments (yellow arrows) extending from the presynaptic membrane. The postsynaptic membrane is marked by dotted lines (cyan). (Scale bar in *E* is 50 nm for all EM virtual images. The models are to the same scale but are slightly rotated for ease of visualization, and the white 50-nm scale bar in *D* is for *D* and *H*, while the white 50-nm scale bar in *I* is for *I–L*.) (*A–D*) Control synapses: Virtual images of docked (*A* and *B*, purple arrows) and nondocked (*C*, blue arrowhead) synaptic vesicles at the presynaptic membrane. Virtual section thickness is 0.35 nm. (*D*) Representative 3D surface model of a control active zone showing one docked vesicle (purple), four nondocked vesicles (blue), and associated tethering filaments (yellow). (*E–H*) LTP synapses: Virtual images of docked (*A* and *B*, purple arrows) and nondocked (*C*, blue arrowhead) synaptic vesicles at the presynaptic membrane. Virtual section thickness is 0.27 nm. (*H*) Representative 3D surface model of a control active zone showing one docked vesicle (purple), four nondocked vesicles (blue), and associated tethering filaments (yellow). (*I–L*) Representative surface models of presynaptic membranes (silver) superimposed with projections from tightly docked vesicles (purple) at (*I*) control and (*K*) LTP synapses, or loosely docked (dark blue) and nondocked (light blue) vesicles at (*J*) control and (*L*) LTP synapses. An unbiased sampling density was computed per 0.01 μm$^2$ of presynaptic membrane surface area by counting all vesicles having projections contained within the rectangle or touching the green inclusion lines, and not counting vesicles touching the red exclusion lines. (*M*) Synaptic vesicle projection densities (control: blue, $n = 22$ synapses; LTP: red, 19 synapses). The density of docked vesicles was greater for LTP than control synapses (KS test, $P = 0.02$). The densities of loosely docked and nondocked vesicles were not significantly different between LTP and control synapses (KS test, $P$ values listed). (*N*) Cumulative frequency plots of distances from loosely docked synaptic vesicles to the presynaptic membrane (SV–PM, KS test, $P = 0.59$) and from nondocked synaptic vesicles to the presynaptic membrane (SV–PM, KS test, $P = 0.56$). (*Inset*: red arrow shows how the distance from SV to the PM was measured.)
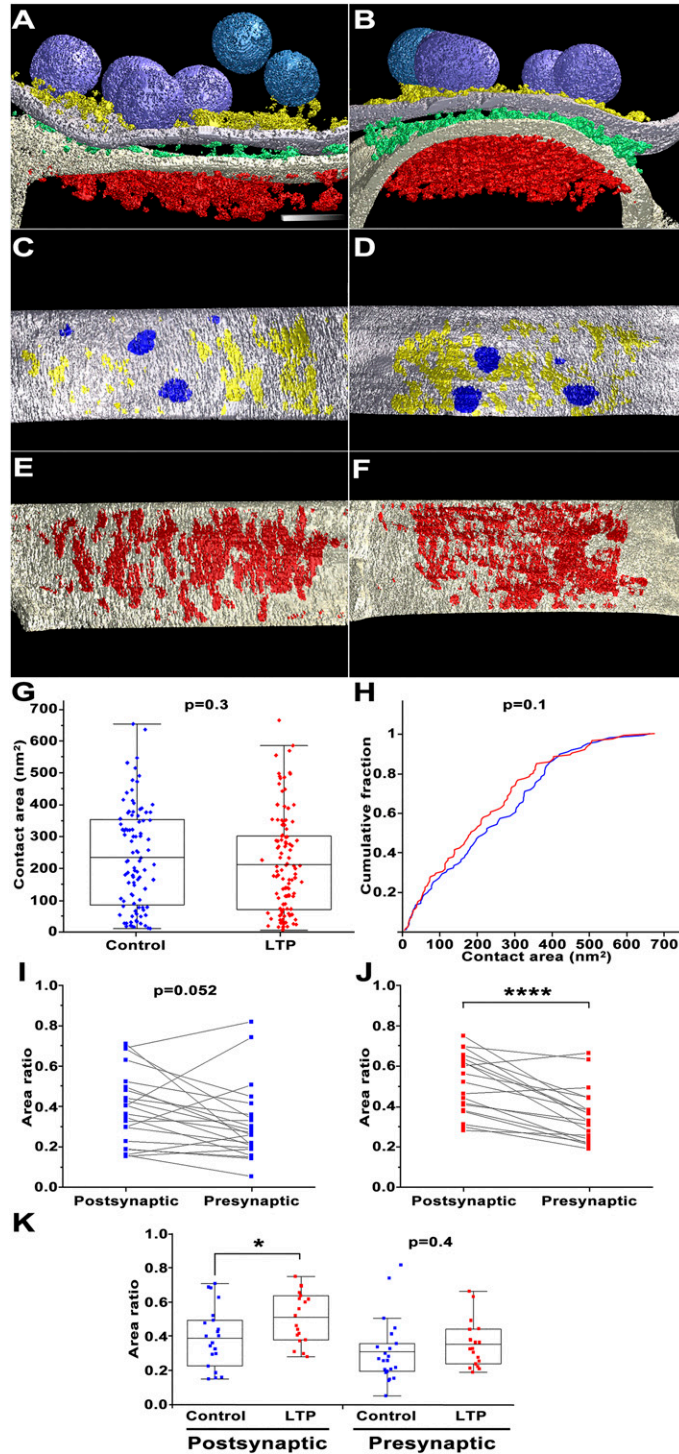
**Fig. 2.** Vesicle contact area and filament occupancy of synaptic membranes. (*A* and *B*) Three-dimensional models of control (*A*) and LTP (*B*) synapses illustrate multiple filaments at the presynaptic membrane (yellow), in the synaptic cleft (green), and at the cytosolic face of the postsynaptic membrane (red). (The slightly rotated 50-nm scale bar in *A* is for *A–F*.) (*C* and *D*) Three-dimensional synapse models of presynaptic membranes from *A* and *B* rotated 90° to reveal filament (yellow) and vesicle contact areas (dark blue) for control (*C*) and LTP (*D*) synapses. (*E* and *F*) Three-dimensional synapse models of postsynaptic membranes from *A* and *B* rotated 90° to reveal postsynaptic filaments (red) for control (*E*) and LTP (*F*) synapses. (*G* and *H*) Scatter plots with box plots (*G*) and cumulative frequency plots (*H*) of docked vesicle contact areas with the presynaptic membrane from control (blue; $n = 96$ vesicles) and LTP (red; $n = 111$ vesicles) synapses. The mean contact areas (control, $240 \pm 160$ nm$^2$; LTP, $210 \pm 160$ nm$^2$) and overall distributions did not differ (*t* test, $P = 0.31$; KS test, $P = 0.14$). (*I* and *J*) Plots for pairs of relative filament occupancy (area ratio) on postsynaptic and presynaptic membranes of control (*I*; $n = 22$) and LTP (*J*; $n = 19$) synapses. Area ratio was calculated by dividing the total filament contact area by the imaged presynaptic or postsynaptic membrane area of each synapse. The contact area of the docked vesicles was subtracted from the total imaged presynaptic membrane area. The relative occupancy (area ratio) of filaments on the postsynaptic membrane was greater than on the presynaptic membrane for LTP synapses (*J*: $0.36 \pm 0.12$, *t* test, $P = 3.3 \times 10^{-5}$), but not control synapses (*I*: $0.31 \pm 0.19$, *t* test, $P = 0.052$). (*K*) The area ratio of filaments on the postsynaptic membrane was greater with LTP (*t* test, $P = 0.021$), but was not different on the presynaptic membrane (*t* test, $P = 0.39$).

Jung et al.
Shortened tethering filaments stabilize presynaptic vesicles in support of elevated release
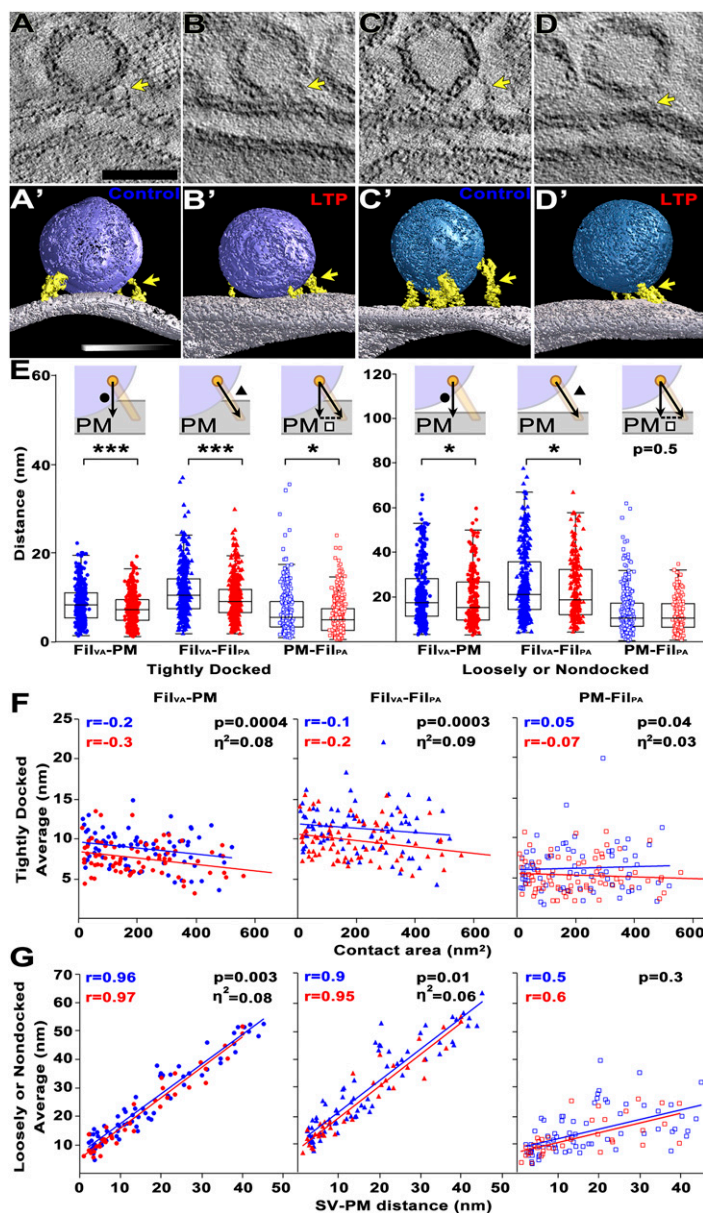probability during LTP in rat hippocampus

**Fig. 3.** Shortened distances between tethering filaments and presynaptic membranes of the active zone following LTP. Virtual sections and surface models of tightly docked vesicles in control (*A* and *A'*, purple) and LTP (*B* and *B'*, purple) conditions and nondocked vesicles in control (*C* and *C'*, blue) and LTP (*D* and *D'*, blue) conditions. The virtual images are 0.35 nm thick for the control synapses (*A* and *C*) and 0.27 nm thick for the LTP synapses (*B* and *D*). Tethering filaments have matching arrows in the virtual sections and surface models (yellow). (Scale bar: 50 nm; in *A* for *A–D* and in *A'* for the 3D models with slight rotation.) (*E*) Three distances were measured separately for every tethering filament on tightly docked and loosely or nondocked vesicles that were incomplete or complete in these EMT samples (see Table 1 for *n* values in each category). Distance was measured between the filament attachment site on the vesicle (Fil$_{VA}$) projected onto the presynaptic membrane (PM) (closed circle and black arrow in the *Insets*). Distance was measured between the Fil$_{VA}$ and its filament attachment site on the presynaptic membrane (Fil$_{PA}$, closed triangle and black arrow in the *Insets*). The distance between these projections along the active zone membrane was calculated assuming a right triangle (PM–Fil$_{PA}$, open square and dotted line in the *Insets*). For tightly docked vesicles, all three values were shorter after LTP relative to control stimulation (Fil$_{VA}$–PM, control = 8.5 ± 4.1 nm and LTP = 7.3 ± 3.5 nm, KS test, *P* = 0.0001; Fil$_{VA}$–Fil$_{PA}$, control = 11 ± 5.5 nm and LTP = 9.5 ± 4.5 nm, KS test, *P* = 0.0001, and PM–Fil$_{PA}$, control = 6.6 ± 4.9 nm and LTP = 5.5 ± 3.9 nm, KS test, *P* = 0.017). For loosely docked or nondocked vesicles, the Fil$_{VA}$–PM and Fil$_{VA}$–Fil$_{PA}$ distances were both shortened after LTP compared to control conditions (Fil$_{VA}$–PM: control, 21 ± 13 nm, and LTP, 19 ± 12 nm; KS test, *P* = 0.042; and Fil$_{VA}$–PM$_{PA}$: control, 26 ± 15 nm, and LTP, 23 ± 13 nm; KS test, *P* = 0.039); however, the calculated PM–Fil$_{PA}$ was not significantly different between conditions (13 ± 9.6 and 12 ± 7.4 nm; KS test, *P* = 0.46). (*F*) Tethering filament distances were averaged for every tightly docked vesicle that was complete in the EMT series and compared to the contact area of the docked vesicle with the presynaptic membrane. These distances were very slightly shorter at larger contact areas for both control and LTP conditions (see *r* values on graphs). The average Fil$_{VA}$–PM, Fil$_{VA}$–Fil$_{PA}$, and PM–Fil$_{PA}$ distances were significantly shorter across the full range of contact areas in the LTP than control synapses (ANCOVA results are on the graphs; for Fil$_{VA}$–PM, *F* = 13, *P* = 0.0004, for Fil$_{VA}$–Fil$_{PA}$, *F* = 14, *P* = 0.0003, and for PM–Fil$_{PA}$, *F* = 4, *P* = 0.04). (*G*) Tethering filament distances were averaged for every loosely docked or nondocked vesicle that was complete in the EMT series and compared to the synaptic vesicle's distance from the presynaptic membrane (SV–PM). The average distances of Fil$_{VA}$–PM, Fil$_{VA}$–Fil$_{PA}$, and PM–Fil$_{PA}$ were highly positively correlated with the SV–PM distance (for control, Fil$_{VA}$–PM, *P* = 9 × 10$^{-42}$, Fil$_{VA}$–Fil$_{PA}$, *P* = 9 × 10$^{-31}$, PM–Fil$_{PA}$, *P* = 9 × 10$^{-7}$; and for LTP, Fil$_{VA}$–PM, *P* = 9 × 10$^{-23}$, Fil$_{VA}$–Fil$_{PA}$, *P* = 2 × 10$^{-19}$, and PM–Fil$_{PA}$, *P* = 2 × 10$^{-5}$). ANCOVA revealed Fil$_{VA}$–PM distances were shorter after LTP (*F* = 10, *P* = 0.003) as was the Fil$_{VA}$–Fil$_{PA}$ (*F* = 7, *P* = 0.01). However, the PM–Fil$_{PA}$ was not significantly reduced after LTP (*F* = 1, *P* = 0.3).

Jung et al.
Shortened tethering filaments stabilize presynaptic vesicles in support of elevated release
probability during LTP in rat hippocampus

PNAS | 5 of 8
https://doi.org/10.1073/pnas.2018653118

**Table 1. Number of objects used for each measurement**

| Measure | Control | LTP | Figures |
|---|---|---|---|
| Active zones imaged | 22 | 19 | 1–3 |
| Tightly docked vesicles in the unbiased sample, including partial vesicles within the inclusion zones | 81 | 97 | 1M |
| Nondocked or (loosely docked) vesicles in the unbiased sample, including partial vesicles within the inclusion zones | 58 (26) | 37 (24) | 1 M and N |
| Tightly docked vesicles with complete contact sites, including vesicles that touched an exclusion plane | 96 | 111 | 2 G–K |
| Filaments on all tightly docked vesicles | 378 | 419 | 3E |
| Filaments on all nondocked or (loosely docked) vesicles | 206 (158) | 93 (117) | 3E |
| Complete tightly docked vesicles | 74 | 78 | 3F |
| Complete nondocked or (loosely docked) vesicles | 48 (25) | 20 (16) | 3G |
| Filaments per complete tightly docked vesicle | 2–10 | 2–11 | 3F |
| Filaments per complete nondocked or (loosely docked) vesicle | 2–10 (2–14) | 2–4 (2–7) | 3G |

as LTP lasts; however, the increase in quantal amplitude returns to baseline by 1 h (14). One model suggests that the transient change in quantal amplitude would occur if vesicle fusion transitioned from kiss-and-run to full fusion (31, 32). The kiss-and-run mode involves a transient formation of a pore between the presynaptic vesicle and active zone membrane. A small amount of neurotransmitter is released before the pore closes, leaving an intact vesicle. Full fusion occurs when a docked and primed vesicle collapses into the presynaptic membrane, releasing all its neurotransmitter in the process. Larger contact areas between a vesicle and presynaptic membrane are consistent with the full fusion mode (20, 33). The kiss-and-run mode is thought to dominate during baseline activity while full fusion has been associated with synaptic plasticity. Pores are so transient that none were captured in these EMT images. Nevertheless, since contact areas did not differ between control and 2-h LTP conditions, it is likely that the mode of vesicle fusion had returned to the baseline kiss-and-run mode.



**Fig. 4.** Modeling effects of LTP on synaptic vesicles and tethering filaments. Tightly docked and loosely or nondocked synaptic vesicles (SV; purple) have filaments (gold) tethering them to the presynaptic membrane (PM; gray). By 2 h following the induction of LTP, the density of tightly docked vesicles nearly doubles. For all three vesicle locations, the attachment sites are displaced lower (vertical dotted arrows) and the filaments become shorter (angled dotted arrows). For the tightly docked vesicles, the attachments sites on the presynaptic membrane shift closer to the vesicle (horizontal arrowheads).

The relative amount of presynaptic membrane area occupied by filaments 2 h after LTP was comparable to control. However, the relative postsynaptic area occupied by filaments increased. Previous work showed that nascent zones, regions containing PSD but lacking presynaptic vesicles, grew by 2 h after LTP induction (30). Modeling predicts the probability of glutamate activating an AMPAR directly beneath a vesicle release site is 0.40 but is drastically reduced to 0.01 when the AMPAR is located 200 nm away from the center of release (34). Therefore, nascent zones added during late-phase LTP are likely to be functionally "silent." These outcomes explain why the excitatory postsynaptic potential does not continue to increase beyond that achieved at LTP induction, despite subsequent growth of the PSD. Taken together, these data indicate that lasting increases in release probability are not likely due to addition of new presynaptic release sites.

Tethering filaments were shortened after LTP, and their attachment sites on vesicles shifted toward the presynaptic membrane. The movement of vesicle and presynaptic filament attachment sites with LTP suggests that the shortening of filaments applies a physical tension between the two sites, ultimately drawing the vesicles closer to the presynaptic membrane. The tethering filaments might comprise any number of proteins engaged in the recruitment, docking, and priming of synaptic vesicles. Assembly of the SNARE complex is required for synaptic vesicle docking and priming (27, 35). One model suggests that docking and priming are not static states, but rather vesicles can oscillate between these states depending on the extent of SNARE complex zippering (27). In this model, docking is defined as the vesicle and presynaptic membrane coming within 8 nm of each other (27), where SNAREs have been shown to form complexes (25, 26). These complexes are visualized as tethering filaments on docked vesicles in EMT. Vesicles transition to a tightly docked state when they come into contact with the presynaptic membrane (19, 36). This tightly docked state is interpreted as the anatomical correlate of vesicle priming (27). Mutations in the $Ca^{2+}$ binding domains of Synaptotagmin-1 reduce the tight docking state, indicating that tight docking is $Ca^{2+}$ dependent (36). Other proteins that might comprise the priming filaments include Munc13-1, Munc18-1, and the CAPS family of proteins, all of which stabilize vesicles in the primed state (29, 37, 38). Rab3-interacting molecule (RIM) mediates the interaction of synaptic vesicles with calcium channels embedded in the presynaptic membrane and has also been identified as a tethering filament (18, 39). In all cases, the shortening or zippering of these candidate tethering molecules could enhance the probability of neurotransmitter release. These studies all took place on the second or millisecond timescale in response to elevated intracellular calcium (38), single or paired action potentials (36), or short-term plasticity induced by high-frequency stimulation (29, 37). The shifted attachment sites shown in our EMT provide ultrastructural evidence that
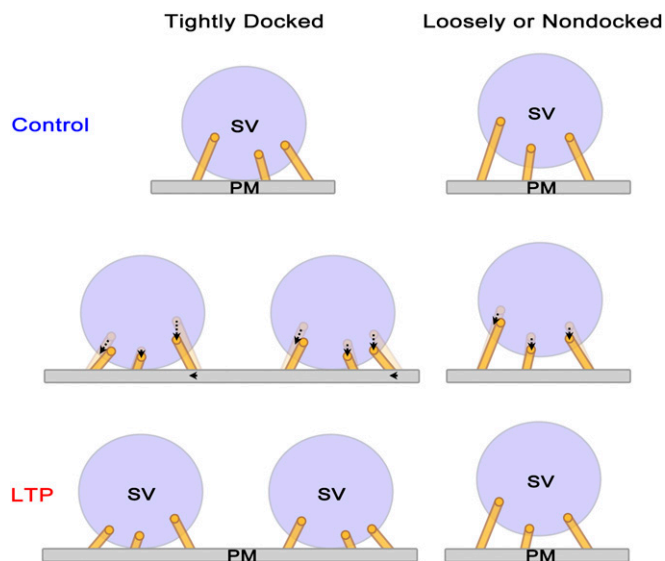
similar mechanisms could still be at play hours after high-frequency stimulation.

In the past, rapid freezing and freeze-substitution have been used to capture ultrastructural changes during synaptic transmission (19, 21, 23, 40–43). Here microwave-enhanced aldehyde fixation of brain slices likely occurs over seconds rather than the millisecond timescale achieved with freezing (44). Aldehyde fixation does not alter the probability of vesicular release recorded in cultured hippocampal neurons (45). Furthermore, similar tethering filaments have been observed in both aldehyde-fixed and rapid frozen synapses (20). Relative to perfusion fixation in vivo, the effects of slicing on presynaptic release are resolved within an hour of incubation in vitro (46), while the LTP effects were measured after ∼6 h in vitro. Any other effects related to the time in vitro were controlled for by test pulse stimulation in the same slice. Hence, we conclude that these observations faithfully reflect a new form of plasticity that underlies a sustained elevation in the probability of release long after the induction of LTP.

Current EMT field size limits investigation to small parts of the synapse at the required high resolution. Hence, we targeted vesicle-rich regions in the middle of the synapse. Whether tether attachment sites shift to bring vesicles closer to the active zone at the edges of synapses or other parts of the presynaptic membrane remains an open question. Presynaptic mitochondria support greater vesicular release at tonic versus phasic synapses (47). Mitochondria-containing boutons sustain a greater loss of synaptic vesicles during LTP than boutons lacking mitochondria (16). None of our EMT volumes were large enough to capture presynaptic mitochondria; hence the outcomes likely include boutons both with or without mitochondria and dilute any mitochondria-specific effects. Combining EMT with wide-field scanning electron microscopy is needed to elucidate nanoscale effects of synaptic plasticity across whole synapses and networks (48).

In summary, the shortening of tethering filaments is likely stabilizing more vesicles in the primed state long after the induction of LTP. Primed vesicles comprise the readily releasable pool, releasing neurotransmitter upon the next action potential. Hence, stabilizing vesicles in the primed state could contribute to the enhanced probability of release occurring several hours after LTP induction.

## Materials and Methods

**Tissue Preparation.** Hippocampal slices, 400 μm thick, were prepared from male Long–Evans rats aged 51 to 65 d (weighing 219 to 361 g). All procedures were approved by the Institutional Animal Care and Use Committees at University of Texas at Austin and Texas A&M University at College Station and described in detail in other studies (15, 20). The animals were anesthetized with halothane and decapitated, and slices were rapidly chopped from the middle one-third of the hippocampus and recovered at 32 °C for 3 h prior to stimulation. A single recording electrode was positioned in the middle of the stratum radiatum midway between two concentric bipolar stimulating electrodes (Fred Haer; 100 μm outside diameter). The stimulating electrodes were separated by 600 to 800 μm to ensure site-specific LTP (15). Baseline and test pulse stimulations were alternated between the control and the LTP electrode once every 2 min with a 30-s interval between electrodes. Theta-burst stimulation (TBS) (eight trains of 10 bursts at 5 Hz of four pulses at 100 Hz delivered 30 s apart) was delivered to one stimulating electrode at time 0 min. Test pulses were delivered to each electrode for ∼30 min prior to TBS to ensure a stable baseline. Responses to test pulses were monitored at both control and LTP sites for 2 h after delivery of the first TBS train. The slices were then fixed by immersion in mixed aldehydes (6% glutaraldehyde and 2% paraformaldehyde in 100 mM cacodylate buffer with 2 mM $CaCl_2$ and 4 mM $MgSO_4$) in the presence of microwave irradiation, and postfixed in the same fixative overnight at room temperature (44). After fixation, slices were stained with 1% osmium tetroxide in a 100 mM cacodylate buffer, embedded in LX-112 (15, 20). Two blocks from one of these slices, one each from the control and LTP sites, were selected for ultrathin sectioning (∼100 nm thick). The thin sections were poststained with saturated uranyl acetate and lead citrate for electron tomography.

**Electron Tomography.** We imaged 41 synapses from the control and LTP sites (Table 1). These tomograms were obtained using FEI Tecnai G2 F20 electron microscope (FEI Company) equipped with a 2,048 × 2,048 Gatan CCD (Gatan) designed for automatic data acquisition. The stage was cooled to liquid $N_2$ temperature to reduce beam damage to the specimen. Each dataset consisted of images taken at 1° tilt interval to about ±60° along a single tilt axis. The tilt images were aligned automatically using 5- or 10-nm gold colloids (British Biocell International) deposited on one or both sides of the sections as fiducial markers before imaging. Alignment of each set of tilt images and volume reconstruction of the images were carried out by using the unified software package for electron tomography, EM3D (em3d.org). The reconstructed volume is composed of small isotropic cubes, namely, voxels. The voxel lengths ranged from 0.27 to 0.54 nm (i.e., 0.02 to 0.16 $nm^3$ per voxel). Virtual slices through the reconstructed volume are one voxel thick. Structures segmented from the reconstruction volumes as virtual slices were examined using EM3D to define individual volumes of interest and they were rendered to generate 3D surface models.

**Electron Tomographic Data Analysis.**
*Distance between vesicle and presynaptic membrane.* The nearest distance was obtained from the surface model of the vesicle to the surface model of the presynaptic membrane. Although several vesicles were incomplete in their reconstructed volume, this distance could be measured for all of the vesicles. *Unbiased density of docked and nondocked vesicles.* The unbiased densities of docked and nondocked vesicles were determined by counting all vesicles with projections that were contained within the rectangle or touching the green inclusion lines. Vesicles touching the red exclusion lines were not counted. The counts were divided by the surface area of the presynaptic membrane to calculate the density or the count per square nanometer. *Contact area of a vesicle with the presynaptic membrane.* The extent of the contact area was measured as described in a previous study (20). The vertices at the interface of the vesicle membrane and presynaptic membrane at their contact site were projected onto the best-fit plane along an eigenvector containing the least eigenvalue. This eigenvalue was calculated using the covariance matrix of the vertices' coordinates. The best-fit plane was pixelated, and each pixel was standardized to have the area of one face of a voxel from the reconstruction to maintain scale. The contact area was calculated by counting the number of pixels that contained the projected vertices and multiplying times pixel size. *Distances between filament attachment sites and the presynaptic membrane (Fig. 3 E, Insets).* The distance from a filament attachment site on the vesicle to the presynaptic membrane ($Fil_{VA}$–PM) was measured as described in previous studies (20, 49). Filament attachment sites were defined at vertices of the interface between surface models of a filament and its associated vesicle membrane. Then the distances were computed from each vertex of a filament attachment site to the closest vertex of the presynaptic membrane and averaged within each filament attachment site. Similarly, the distance was measured between a filament attachment site on the vesicle and the attachment site on the presynaptic membrane ($Fil_{VA}$–$Fil_{PA}$). The distance between $Fil_{VA}$–PM and $Fil_{VA}$–$Fil_{PA}$ was calculated by taking the square root of the subtraction of the squared distance of $Fil_{VA}$–PM from the squared distance of $Fil_{VA}$–$Fil_{PA}$ (PM–$Fil_{PA}$). *Areas and relative areas.* For each tomogram, we counted the total number of voxels located within one voxel length of the presynaptic or postsynaptic membrane. This count was multiplied by the area of one voxel face to determine the total area of the imaged presynaptic or postsynaptic membranes. The relative areas of filament–membrane contact sites were calculated by determining the total number of voxels the filaments occupied and then dividing by the total imaged presynaptic or postsynaptic membrane, respectively. *Statistical analyses.* The distributions of data were tested with the KS normality test. When the distributions satisfied this normality test, Student's $t$ tests (two-tailed) were used to test for significant differences. Data with nonnormal distributions were tested by nonparametric methods (KS test). Analyses of covariance (ANCOVAs) were performed to determine whether LTP significantly altered key relationships, as indicated in the figures. In each case, homogeneity of slopes and correlations were tested prior to ANCOVA. In all analyses, significance was defined as $P < 0.05$. Eta-squared ($\eta^2$) was computed to assess effect sizes. Nonparametric distributions of the data are expressed as scatter plots and box plots with medians and SDs and normal data as scatter plots with box plots, means, and SDs. All the statistical analyses were performed with OriginPro (OriginLab), MATLAB (MathWorks), or IDL (Interactive Data Language; Exelis Visual Information Solutions).

NEUROSCIENCE

Jung et al.
Shortened tethering filaments stabilize presynaptic vesicles in support of elevated release probability during LTP in rat hippocampus

PNAS | 7 of 8
https://doi.org/10.1073/pnas.2018653118

1. T. V. Bliss, A. R. Gardner-Medwin, Long-lasting potentiation of synaptic transmission in the dentate area of the unanaestetized rabbit following stimulation of the perforant path. *J. Physiol.* **232**, 357–374 (1973).
2. R. A. Nicoll, A brief history of long-term potentiation. *Neuron* **93**, 281–290 (2017).
3. J. Larson, G. Lynch, Induction of synaptic potentiation in hippocampus by patterned stimulation involves two events. *Science* **232**, 985–988 (1986).
4. P. V. Nguyen, E. R. Kandel, Brief theta-burst stimulation induces a transcription-dependent late phase of LTP requiring cAMP in area CA1 of the mouse hippocampus. *Learn. Mem.* **4**, 230–243 (1997).
5. U. Staubli, G. Lynch, Stable hippocampal long-term potentiation elicited by "theta" pattern stimulation. *Brain Res.* **435**, 227–234 (1987).
6. G. Capocchi, M. Zampolini, J. Larson, Theta burst stimulation is optimal for induction of LTP at both apical and basal dendritic synapses on hippocampal CA1 neurons. *Brain Res.* **591**, 332–336 (1992).
7. T. V. Bliss, T. Lomo, Long-lasting potentiation of synaptic transmission in the dentate area of the anaesthetized rabbit following stimulation of the perforant path. *J. Physiol.* **232**, 331–356 (1973).
8. T. V. Bliss, G. L. Collingridge, A synaptic model of memory: LTP in the hippocampus. *Nature* **361**, 31–39 (1993).
9. D. M. Kullmann, R. A. Nicoll, Long-term potentiation is associated with increases in quantal content and quantal amplitude. *Nature* **357**, 240–244 (1992).
10. D. Liao, A. Jones, R. Malinow, Direct measurement of quantal changes underlying long-term potentiation in CA1 hippocampus. *Neuron* **9**, 1089–1097 (1992).
11. C. Stricker, A. C. Field, S. J. Redman, Changes in quantal parameters of EPSCs in rat CA1 neurones in vitro after the induction of long-term potentiation. *J. Physiol.* **490**, 443–454 (1996).
12. C. F. Stevens, Y. Wang, Changes in reliability of synaptic function as a mechanism for plasticity. *Nature* **371**, 704–707 (1994).
13. R. Malinow, R. W. Tsien, Presynaptic enhancement shown by whole-cell recordings of long-term potentiation in hippocampal slices. *Nature* **246**, 170 (1973).
14. M. V. Sokolov, A. V. Rossokhin, A. V. Astrelin, J. U. Frey, L. L. Voronin, Quantal analysis suggests strong involvement of presynaptic mechanisms during the initial 3 h maintenance of long-term potentiation in rat hippocampal CA1 area in vitro. *Brain Res.* **957**, 61–75 (2002).
15. J. N. Bourne, K. M. Harris, Coordination of size and number of excitatory and inhibitory synapses results in a balanced structural plasticity along mature hippocampal CA1 dendrites during LTP. *Hippocampus* **21**, 354–373 (2011).
16. H. L. Smith et al., Mitochondrial support of persistent presynaptic vesicle mobilization with age-dependent synaptic growth after LTP. *eLife* **5**, 1–30 (2016).
17. R. Fernández-Busnadiego et al., Quantitative analysis of the native presynaptic cytomatrix by cryoelectron tomography. *J. Cell Biol.* **188**, 145–156 (2010).
18. R. Fernández-Busnadiego et al., Cryo-electron tomography reveals a critical role of RIM1α in synaptic vesicle tethering. *J. Cell Biol.* **201**, 725–740 (2013).
19. C. Imig et al., The morphological and molecular nature of synaptic vesicle priming at presynaptic active zones. *Neuron* **84**, 416–431 (2014).
20. J. H. Jung, J. A. Szule, R. M. Marshall, U. J. McMahan, Variable priming of a docked synaptic vesicle. *Proc. Natl. Acad. Sci. U.S.A.* **113**, E1098–E1107 (2016).
21. G. A. Zampighi, R. Serrano, J. L. Vergara, A novel synaptic vesicle fusion path in the rat cerebral cortex: The "saddle" point hypothesis. *PLoS One* **9**, e100710 (2014).
22. L. Siksou et al., Three-dimensional architecture of presynaptic terminal cytomatrix. *J. Neurosci.* **27**, 6868–6877 (2007).
23. A. A. Cole, X. Chen, T. S. Reese, A network of three types of filaments organizes synaptic vesicles for storage, mobilization, and docking. *J. Neurosci.* **36**, 3222–3230 (2016).
24. S. Nagwaney et al., Macromolecular connections of active zone material to docked synaptic vesicles and presynaptic membrane at neuromuscular junctions of mouse. *J. Comp. Neurol.* **513**, 457–468 (2009).
25. H. Yavuz et al., Arrest of *trans*-SNARE zippering uncovers loosely and tightly docked intermediates in membrane fusion. *J. Biol. Chem.* **293**, 8645–8655 (2018).
26. F. Li et al., Energetics and dynamics of SNAREpin folding across lipid bilayers. *Nat. Struct. Mol. Biol.* **14**, 890–896 (2007).
27. E. Neher, N. Brose, Dynamically primed synaptic vesicle states: Key to understand synaptic short-term plasticity. *Neuron* **100**, 1283–1291 (2018).
28. R. B. Sutton, D. Fasshauer, R. Jahn, A. T. Brunger, Crystal structure of a SNARE complex involved in synaptic exocytosis at 2.4 Å resolution. *Nature* **395**, 347–353 (1998).
29. E. He et al., Munc13-1 and Munc18-1 together prevent NSF-dependent de-priming of synaptic vesicles. *Nat. Commun.* **8**, 15915 (2017).
30. M. E. Bell et al., Dynamics of nascent and active zone ultrastructure as synapses enlarge during long-term potentiation in mature hippocampus. *J. Comp. Neurol.* **522**, 3861–3884 (2014).
31. J. Lisman, S. Raghavachari, A unified model of the presynaptic and postsynaptic changes during LTP at CA1 synapses. *Sci. STKE* **2006**, re11 (2006).
32. S. Choi, J. Klingauf, R. W. Tsien, Fusion pore modulation as a presynaptic mechanism contributing to expression of long-term potentiation. *Philos. Trans. R. Soc. Lond. B Biol. Sci.* **358**, 695–705 (2003).
33. R. Long, C. Y. Hui, A. Jagota, M. Bykhovskaia, Adhesion energy can regulate vesicle fusion and stabilize partially fused states. *J. R. Soc. Interface* **9**, 1555–1567 (2012).
34. K. M. Franks, C. F. Stevens, T. J. Sejnowski, Independent sources of quantal variability at single glutamatergic synapses. *J. Neurosci.* **23**, 3186–3195 (2003).
35. J. H. Jung, S. Doniach, A stochastic model of active zone material mediated synaptic vesicle docking and priming at resting active zones. *Sci. Rep.* **7**, 278 (2017).
36. S. Chang, T. Trimbuch, C. Rosenmund, Synaptotagmin-1 drives synchronous $Ca^{2+}$-triggered fusion by $C_2B$-domain-mediated synaptic-vesicle-membrane attachment. *Nat. Neurosci.* **21**, 33–40 (2018).
37. W. J. Jockusch et al., CAPS-1 and CAPS-2 are essential synaptic vesicle priming proteins. *Cell* **131**, 796–808 (2007).
38. Y. Lai et al., Molecular mechanisms of synaptic vesicle priming by Munc13 and Munc18. *Neuron* **95**, 591–607.e10 (2017).
39. D. Sarkar et al., Expansion revealing: Decrowding proteins to unmask invisible brain nanostructures. *bioRxiv* [Preprint] (2020). https://www.biorxiv.org/content/10.1101/2020.08.29.273540v1 (Accessed 1 September 2020).
40. J. Heuser, T. Reese, M. Dennis, Synaptic vesicle exocytosis captured by quick freezing and correlated with quantal transmitter release. *J. Cell Biol.* **81**, 275–300 (1979).
41. S. Watanabe et al., Ultrafast endocytosis at mouse hippocampal synapses. *Nature* **504**, 242–247 (2013).
42. S. Watanabe et al., Clathrin regenerates synaptic vesicles from endosomes. *Nature* **515**, 228–233 (2014).
43. G. A. Zampighi et al., Conical electron tomography of a chemical synapse: Polyhedral cages dock vesicles to the active zone. *J. Neurosci.* **28**, 4151–4160 (2008).
44. F. E. Jensen, K. M. Harris, Preservation of neuronal ultrastructure in hippocampal slices using rapid microwave-enhanced fixation. *J. Neurosci. Methods* **29**, 217–230 (1989).
45. J. C. Rosenmund, C. F. Stevens, The rate of aldehyde fixation of the exocytotic machinery in cultured hippocampal synapses. *J. Neurosci. Methods* **76**, 1–5 (1997).
46. J. C. Fiala et al., Timing of neuronal and glial ultrastructure disruption during brain slice preparation and recovery in vitro. *J. Comp. Neurol.* **465**, 90–103 (2003).
47. L. Brodin, L. Bakeeva, O. Shupliakov, Presynaptic mitochondria and the temporal pattern of neurotransmitter release. *Philos. Trans. R. Soc. Lond. B Biol. Sci.* **354**, 365–372 (1999).
48. M. Kuwajima, J. M. Mendenhall, L. F. Lindsey, K. M. Harris, Automated transmission-mode scanning electron microscopy (tSEM) for large volume analysis at nanoscale resolution. *PLoS One* **8**, e59573 (2013).
49. J. H. Jung, J. A. Szule, K. Stouder, R. M. Marshall, U. J. McMahan, Active zone material-directed orientation, docking, and fusion of dense core vesicles alongside synaptic vesicles at neuromuscular junctions. *Front. Neuroanat.* **12**, 72 (2018).

**8 of 8** | **PNAS**
https://doi.org/10.1073/pnas.2018653118

**Jung et al.**
Shortened tethering filaments stabilize presynaptic vesicles in support of elevated release probability during LTP in rat hippocampus